Experimental Test of the $1/\tau$-Scaling Entropy Generation in Finite-Time Thermodynamics

Yu-Han Ma,[1,2] Ruo-Xun Zhai,[3,2] Jinfu Chen,[1,2] C. P. Sun,[1,2] and Hui Dong[2,*]
[1]*Beijing Computational Science Research Center, Beijing 100193, China*
[2]*Graduate School of China Academy of Engineering Physics, No. 10 Xibeiwang East Road, Haidian District, Beijing 100193, China*
[3]*Beijing Normal University, Beijing 100875, China*

(Received 5 November 2019; revised 12 February 2020; accepted 7 October 2020; published 19 November 2020)

The finite-time dynamics, apart from its fundamental importance in nonequilibrium thermodynamics, is of great significance in designing heat engine cycles. We build an experimental apparatus to test the predicted long-time $1/\tau$ scaling of the irreversible entropy generation in the finite-time (τ) thermodynamic process by compressing dry air in a temperature-controlled water bath. We present the first direct experimental validation of the scaling, utilized in many finite-time thermodynamic models at the long-time regime. The experimental data also demonstrate a clear deviation from the scaling at the short-time regime. We show the optimal control scheme to minimize the irreversible entropy generation in finite-time process. Such optimization shall bring new insight to the practical design of heat engine cycles.

DOI: 10.1103/PhysRevLett.125.210601

Introduction.—Heat engines, converting heat into useful work, have important practical applications and attract a wide range of research interests in both classical and quantum thermodynamics [1–6]. The Carnot theorem [1] limits the maximum efficiency of heat engines with the well-known Carnot efficiency. Unfortunately, achieving such efficiency is typically accompanied by a vanishing output power due to the infinite long operation time in a quasistatic thermodynamic process [1,7–10]. The futility of the Carnot engine with vanishing power has pushed us to design a finite-time cycle to achieve high efficiency while maintaining the output power [11–16]. And the quantitative evaluation of the irreversibility is the key for such design [6,11,14–20].

The thermodynamics irreversibility is typically quantitatively *evaluated via* irreversible *entropy generation* in both classical and quantum thermodynamics [1–6]. The trade-off relation between power and efficiency [21–24] is significantly determined by the $1/\tau$ scaling of irreversible entropy generation on the long control time τ. Such scaling has been predicted in different finite-time thermodynamic models [25], such as the endoreversible [11,12,26,27], linear [14,19,28,29], stochastic [30–34], and low-dissipation models [16,24,35] for both the classical [12] and quantum system [23,24,36]. Despite great theoretical progresses, direct experimental testing remains lacking due to the unavailability of suitable platforms.

In this Letter, we fill the gap between theory and experiments by designing an apparatus to test such $1/\tau$ scaling of the irreversible entropy generation at the long-time regime by compressing dry air in a temperature-controlled water bath. The utilization of pressure sensors is surprisingly practical despite its extreme simplicity and provides sufficient accuracy for the current measurement. Given this feature, we validate the scaling with enough precision to quantitatively determine the coefficient $\mathcal{C}$ of the scaling, i.e., $\mathcal{C}/\tau$. Further, we verify that the compression with a constant speed is the optimal scheme to minimize the coefficient $\mathcal{C}$ within the set of power control functions to reduce the irreversible entropy generation. Additionally, our experimental results reveal the deviation from the scaling at the short-time regime.

The $1/\tau$ scaling in the ideal gas system.—We first derive the $1/\tau$ scaling for the ideal gas system, which is in contact with a heat bath of constant temperature T_e. The volume V of the gas is tuned from V_0 at $t=0$ to V_f at the end of the process $t=\tau$. Under the endoreversible assumption [11,12,26,27], the irreversible entropy generation is written as [12]

$$\Delta S^{(\mathrm{ir})} = \int_0^\tau \left(\frac{\dot{Q}_s}{T_s} + \frac{\dot{Q}_e}{T_e}\right) dt, \tag{1}$$

where $\dot{Q}_s = -\dot{Q}_e = \delta Q_s/dt$ is the heat flow from the heat bath to the system. The effective temperature $T_s(t)$ of the system generally varies with time t in the control process. In the quasistatic process with infinite control time ($\tau \to \infty$), the system is always in the thermal equilibrium with the bath, namely, $T_s(t) = T_e$. For the long-time τ in comparison with the relaxation time t_r between the gas and the heat bath, the system is in the linear irreversible regime with T_s slightly deviated from the bath temperature, namely, $|T_s(t) - T_e|/T_e \ll 1$. Here, the relaxation time t_r characterizes the time for the system to equilibrate with

the thermal bath and can be experimentally measured. The heat exchange between the system and bath follows Newton's law of cooling as

$$\delta Q_s = -\kappa[T_s(t) - T_e]dt, \tag{2}$$

where κ is the thermal conductance of the system and can be determined by the relaxation time t_r and the heat capacity C_V of the system (see the Supplemental Material [37] for detailed explanation). Combining Eqs. (1) and (2), we obtain the irreversible entropy generation as

$$\Delta S^{(\mathrm{ir})} = \int_0^\tau \kappa \frac{[T_s(t) - T_e]^2}{T_s(t)T_e} dt. \tag{3}$$

For the current dry air system, the irreversible entropy generation under the long-time limit is proportional to the irreversible work $W_{\mathrm{Th}}^{(\mathrm{ir})}$, namely,

$$W_{\mathrm{Th}}^{(\mathrm{ir})} = T_e \Delta S^{(\mathrm{ir})} = \frac{P_0 P_f^{\mathrm{iso}} (V_f - V_0)^2}{\kappa T_e \tau}, \tag{4}$$

where P_0 is the initial pressure of the dry air and P_f^{iso} is the isothermal pressure $P_f^{\mathrm{iso}} = P_0 V_0 / V_f$ of the air at the end of the process. The detailed derivation of the above equation is shown in the Supplemental Material [37]. The relation in Eq. (4) shows the $1/\tau$ scaling for the current dry air system at the long-time τ and also provides the connect between the irreversible entropy generation and the measurable quantity $W_{\mathrm{Th}}^{(\mathrm{ir})}$. Experimentally, such irreversible work $W_{\mathrm{exp}}^{(\mathrm{ir})}(\tau) = W_{\mathrm{exp}}(\tau) - W_q$ is obtained by subtracting the work $W_q = P_0 V_0 \ln(V_0/V_f)$ of the quasistatic isothermal process from the measured work via

$$W_{\mathrm{exp}}(\tau) = -\int_0^\tau P(t)\dot{V}(t)dt. \tag{5}$$

With the experimentally measured pressure P and volume V, we evaluate the work via Eq. (5) and compare it with the theoretical result of Eq. (4). Hereafter, the irreversibility of the current system is measured via the irreversible work [12,17] to validate the scaling and to demonstrate the deviation from the scaling at the short-time regime.

Verification of the $1/\tau$ *scaling.*—To test the scaling with dry air, an apparatus in Fig. 1(a) is designed to measure the state of the dry air, which is sealed in a compressible cylinder (A) and three buffer cylinders (B, C, D). A piston is installed in the cylinder A to compress the air with a computer-controlled stepper motor M. By setting push programs, a controllable change in the volume of the gas over time is achieved, i.e., $V(t) = V_0 - \mathcal{A}L(t)$, where $V_0 = 2.584 \times 10^{-3}$ m^3 is the initial volume of the gas and $\mathcal{A} = 1.963 \times 10^{-3}$ m^2 is the cross-sectional area of the cylinder A. The stepper motor allows us to realize the

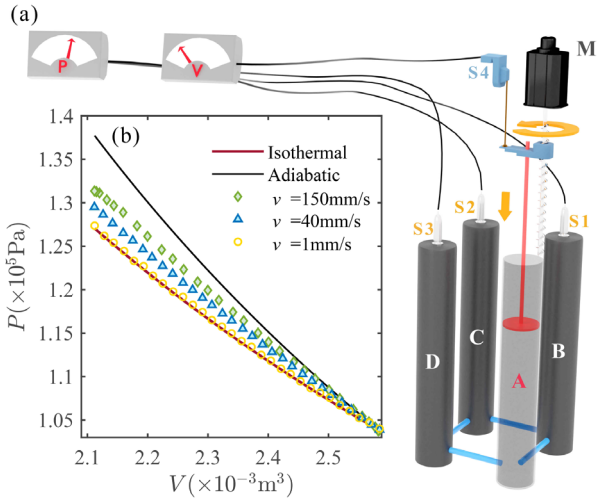

FIG. 1. Experimental setup for measuring irreversible entropy generation in the finite-time quasi-isothermal process. (a) Experimental setup. The dry air is sealed in four connected cylinders A, B, C, and D. The piston A is propelled by the computer-controlled stepper motor M to achieve the controlled compression. Three pressure sensors $S1$, $S2$, and $S3$ are connected to the top of the three cylinders B, C, and D, respectively, to measure the air pressure $P(t)$ in the cylinders. And the displacement of the piston $L(t)$ is detected by a position sensor $S4$ to reveal the gas volume $V(t)$. The cylinders are immersed in the water bath with fixed temperature T_e. (b) $P - V$ diagram of the gas under the bath temperature $T_e = 313.15$ K. The green diamonds, blue triangles, and yellow circles are obtained for the piston speeds $v = 150$, $v = 40$, and $v = 1$ mm/s, respectively. The red solid line represents $P - V$ curve of the theoretical quasistatic isothermal process, namely, $PV = \mathrm{const}$, while the black solid line, i.e., $PV^\gamma = \mathrm{const}$, corresponded to the adiabatic process. Here, $\gamma = 1.4$ is the heat capacity ratio of the dry air [38].

finite-time quasi-isothermal compression process with different process time τ. To measure the work $W_{\mathrm{exp}}(\tau)$ in Eq. (5), we monitor the gas pressure $P = P(t)$ with three sensors, numbered $S1$, $S2$, and $S3$ (range 0–0.15 MPa, accuracy 0.1%) on the top of the three cylinders B, C, and D, respectively. The volume change $dV = \mathcal{A}dL(t)$ is measured through the piston position $L(t)$ with the sensor $S4$ (range 0–0.3 m, accuracy 0.1%).

In the compression process, the four cylinders are immersed in a water bath with fixed temperature (accuracy 0.5 K). For the gas system, the endoreversible condition [11,12,26,27] ensures the system is in the internal equilibrium and characterized with the effective temperature T_s, known as the endoreversible temperature. Physically, the internal relaxation time of the gas is much smaller than the relaxation time t_r for the gas to equilibrate with the thermal bath. In the current setup, $t_r = 1.94$ s is measured in the experiment, with details explained in the Supplemental Material [37].

The state of the dry air is illustrated via the $P - V$ diagram in Fig. 1(b) with the pressure $P(t)$ measured from the sensor $S1$ and the volume calculated from the sensor $S4$.

The motor is designed to control the piston to move at a constant speed v and the piston displacement at time t is $L(t) = vt$. The total displacement of the piston is $\Delta L = L(\tau) = 240$ mm. In the plot, we show the $P - V$ diagram for the different piston speeds $v = 150$ mm/s (green diamond), $v = 40$ mm/s (blue triangle), and $v = 1$ mm/s (yellow circle). At the low piston speed, the $P - V$ curve approaches that of the quasistatic isothermal process illustrated by the red solid line. At the high piston speed, the $P - V$ curve approaches the one of the adiabatic process marked with the black solid line ($PV^{\gamma} = \text{const}$). Here $\gamma = 1.4$ is the heat capacity ratio for dry air [38]. The data from pressure sensors $S2$ and $S3$ are illustrated in the Supplemental Material [37].

The measured work $W_{\text{exp}}(\tau)$ is illustrated as the function of the process time τ in Fig. 2(a). The red circles and blue diamonds show the measured work at the bath temperature $T_e = 323.15$ and $T_e = 313.15$ K, respectively. Each data point is averaged from 20 repeats. In Fig. 2(a), the measured work approaches a stable value, which matches the work W_q in the quasistatic isothermal process (the dashed line). The work $W_q = P_0 V_0 \ln(V_0/V_f)$ is obtained from the initial pressure P_0, volume V_0, and the final volume V_f. The log-log plot of the irreversible work $W_{\text{exp}}^{(\text{ir})}$ in Figs. 2(b) and 2(c) show the good agreements in the long-time regime of $\tau \gg t_r$ with the theoretical prediction $W_{\text{Th}}^{(\text{ir})}$ in Eq. (4), which is represented by the black solid line. Therefore, we validate the behavior that the entropy generation is inversely proportional to the process time in the long-time regime.

The data also show significant discrepancy between the scaling behavior in Eq. (4) and the experimental data at the short-time regime ($\tau < 10t_r$) in Figs. 2(b) and 2(c). To understand the discrepancy at the short-time regime, we simulate the exact dynamics of the temperature change in Eq. (2) without approximation and calculate the work accordingly. The calculated work is illustrated as functions of the control time τ with dash-dotted lines in the figures. The simulated results match the theoretical equation at the long-time τ. At the short-time regime, the simulated result follows the trend of the data, yet does not match the exact value.

The mismatch between the experimental data and the simulated results is caused by treating the thermal conductance κ as a constant in the simulation [39,40]. We fit the experimentally obtained $P(t)$ curve with the corresponding simulated curve (taking κ as the fitting parameter) for each compression speed v. The fitted value of $\kappa(v)$ increases with the compression speed v (see Supplemental Material [37] for detailed discussion). In the short-time regime, κ is higher than the constant κ_0 we measured with the isochoric relaxation process, and the gas relaxes to the equilibrium state faster with less irreversible work. The irreversible work calculated with the fitted value κ is plotted as dotted lines in Figs. 2(b) and 2(c). The curves with fitted thermal conductance match well with the experimental data.

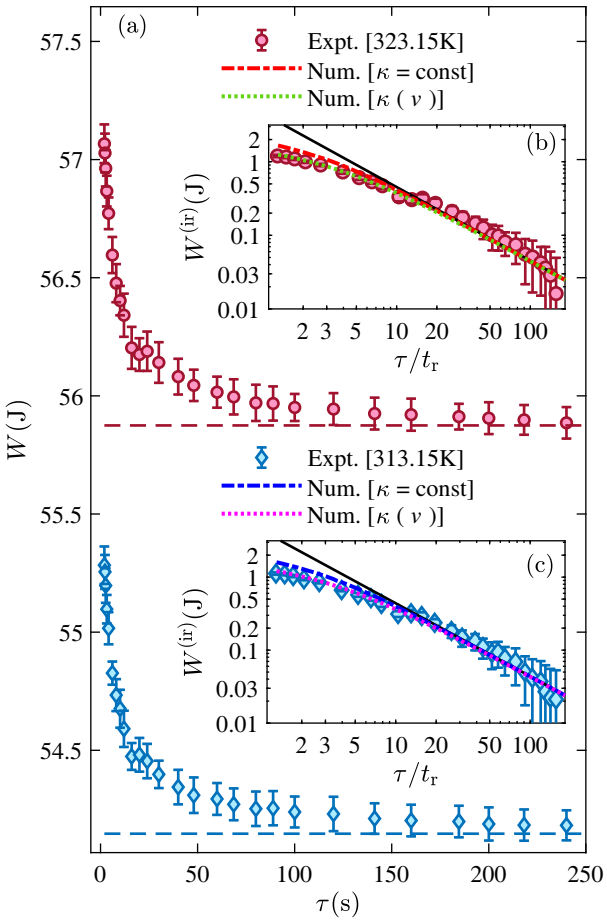

FIG. 2. Work in the finite-time quasi-isothermal process. (a) Work done by the piston onto the gas as the function of the process time τ. The experimental results $W_{\text{exp}}(\tau)$ are illustrated by the red circles and blue diamonds with the corresponding bath temperature $T_e = 323.15$ and $T_e = 313.15$ K, respectively. The work W_q in the quasistatic process is marked by the red (blue) dashed line for $T_e = 323.15(313.15)$ K. The log-log plot of the irreversible work $W_{\text{exp}}^{(\text{ir})}(\tau)$ as the function of dimensionless time τ/t_r is illustrated in (b) with $T_e = 323.15$ K and (c) with $T_e = 313.15$ K. The corresponding theoretical result $W_{\text{Th}}^{(\text{ir})}$ of Eq. (4) is represented by the black solid line. The dash-dotted lines and dotted lines, respectively, show the irreversible work calculated numerically from Eq. (2) with the constant κ_0 and the fitted $\kappa(v)$.

Effect of the control scheme.—With the above compression process at the constant speed, we have validated the $1/\tau$ scaling of the irreversible entropy generation via the measurement of the irreversible work at the long-time limit. As predicted in the previous study [12,36], the coefficient $\mathcal{C}$ in the $\mathcal{C}/\tau$ scaling is not only determined by the parameters of the system and heat bath, but also related to the specific way the system is controlled. In the following experiment, we show the impact of different control schemes on the irreversible work with our setup in a discrete quasi-isothermal process [17].

The discrete quasi-isothermal process, introduced by Andresen *et al.* in Ref. [41], is an effective approach for

optimizing the finite-time Carnot engine. The basic idea of the discrete quasi-isothermal process is to use a series of adiabatic and isochoric processes to approximate the finite-time quasi-isothermal process. And the discrete step processes have been used to study different thermodynamic issues, such as work distribution [42], thermodynamic length [43], and optimization of quantum heat engines [36,44]. We utilize the discrete quasi-isothermal process to take the two advantages. Theoretically, the state of the system can be analytically solved and experimentally the work and the heat exchange happen in different subprocesses to allow direct measurement.

The scheme of the discrete quasi-isothermal process is shown in Fig. 3(a). The piston is rapidly pushed to the position L_i $(i = 1, 2, \ldots, M)$ for the ith step to form an adiabatic process. And then the gas relaxes to thermal equilibrium through the isochoric process with duration $\delta\tau$. The stepper motor is controlled to push the piston to the designed position L_i given by a power function $L_i = (i/M)^{\alpha}\Delta L$ in the ith step. Here α is the index for the realization of different control functions. In Fig. 3(a),

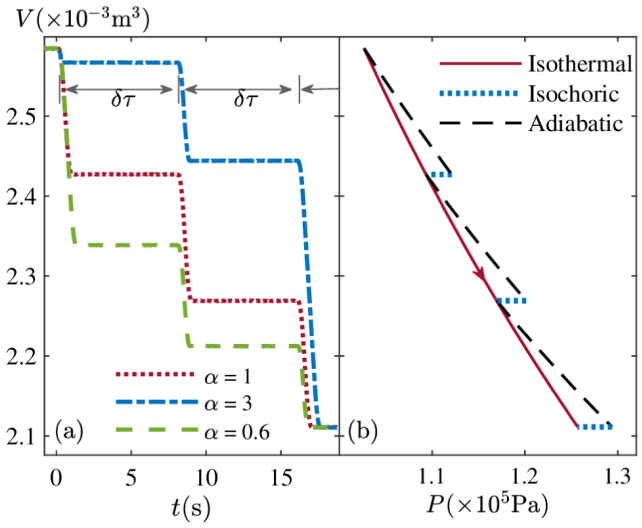

FIG. 3. The volume change and the $P - V$ diagram in the discrete quasi-isothermal process with the three-step case as an example. (a) Volume changes with time in the three-step discrete quasi-isothermal process with different push modes. The step time is $\delta\tau = 8$ s. The piston is pushed to the position $L_i = (i/3)^{\alpha}\Delta L, (i = 1, 2, 3)$ at the end of the ith step. The volume $V_i = V_0 - \mathcal{A}L_i$ with sublinearly ($\alpha = 0.6$), linearly ($\alpha = 1$), and superlinearly ($\alpha = 3$) are illustrated by the green dashed line, red dotted line, and blue dash-dotted line, respectively. (b) $P - V$ diagram of the three-step DIP. Series of adiabatic (black dashed line) and isochoric (blue dotted line) processes are used to approach a finite-time quasi-isothermal process (red solid line). In the ith ($i = 1$, 2, 3) step, the gas volume is first compressed from V_i to V_{i+1} adiabatically, then the gas isochorically relaxes to the thermal equilibrium state with the temperature T_e. The experimental $P - V$ diagram is shown in the Supplemental Material [37].

the green dashed line, red dotted line, and blue dash-dotted line show the volume changes where the piston has been pushed sublinearly $\alpha = 0.6$, linearly $\alpha = 1$, and superlinearly $\alpha = 3$, respectively. The initial (final) piston position is $L_0 = 0$ ($L_M = \Delta L$). For clarity, we show three control schemes with total step number $M = 3$ and duration time $\delta\tau = 8$ s as an example. At the beginning of the each adiabatic process, the gas maintains the same temperature as the water bath, since $\delta\tau$ is larger than the relaxation time t_r that $\exp[-\delta\tau/t_r] \ll 1$. We define the average speed of the piston in one step as $v_i = (L_i - L_{i-1})/\delta\tau$.

For the discrete quasi-isothermal process with $M \gg 1$ steps, the irreversible work of the system is explicitly written as (see Supplemental Material [37] for detailed derivation)

$$W_{\mathrm{Th}}^{(\mathrm{ir})} = \frac{\Lambda\Theta}{M}, \tag{6}$$

where $\Theta = (\gamma - 1)P_0(V_f - V_0)^2/(2V_0)$ shows the dependence on the initial and final state of the system. And $\Lambda = \langle v^2\rangle/\langle v\rangle^2$, characterizing the speed fluctuation of the piston, is determined by the control scheme of the stepper motor with $\langle v^2\rangle \equiv \sum_{i=1}^{M} v_i^2/M$ and $\langle v\rangle = \sum_{i=1}^{M} v_i/M$. With the fixed process time $\tau = M\delta\tau$, any control scheme with the power function [36,45,46] results in $\Lambda \geq 1$.

The change of the control functions are realized with different power indexes α. The schematic $P - V$ curve for the discrete quasi-isothermal process is illustrated in Fig. 3 (b). The irreversible work done in discrete quasi-isothermal process is illustrated in Fig. 4(a) as the function of the total step number M for three different power indexes $\alpha = 0.6$ (green triangle), 1.0 (red circle), and 3.0 (blue diamond). Each data point has been averaged from 20 repeats. The corresponding dashed lines show the fitting with the theoretical result in Eq. (6). At the large M regime, the irreversible work is inversely proportional to M.

To show the dependence of the irreversible work on the control function, we extract the coefficient Λ of the $1/M$ scaling in Eq. (6) by fitting curves in Fig. 4(a) with Eq. (6) for different α at the large step number M, and plot Λ as the function of the index α in Fig. 4(b). The coefficient Λ estimated from the experiments is shown as the red diamonds in Fig. 4(b). The theoretical result of Eq. (6) is shown as the green circles in Fig. 4(b). The figure shows the agreement between the theoretical result and the experimental data. The experimental data demonstrate the minimum irreversible work at the index $\alpha = 1$. We conclude that, within the set of power function, the minimal irreversible work is achieved with the linearly control function [36], namely, $\alpha = 1$ as shown in Fig. 4.

With the dependence of the control function Λ, we can control the irreversible work of the system via different schemes to adjust the power and efficiency of the heat engine [36] in the Carnot-like cycle. Experimentally, such

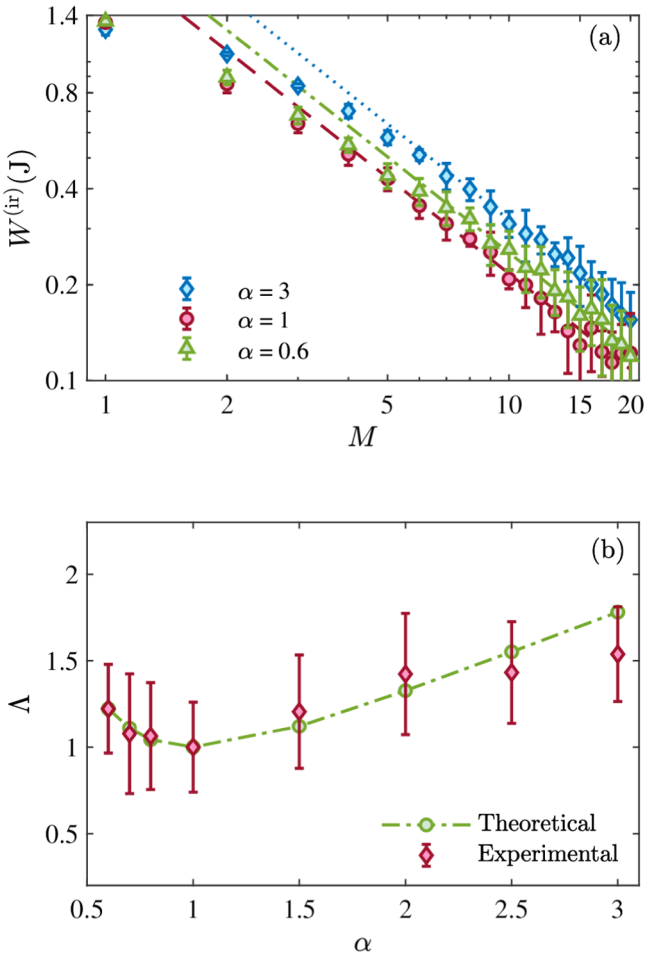

FIG. 4. Irreversible work with different control schemes of the discrete quasi-isothermal process. The temperature of the water bath is $T_e = 313.15$ K. (a) Log-log plot of the irreversible work $W_{\mathrm{exp}}^{(\mathrm{ir})}$ as the function of step number M. We demonstrate the $1/M$ scaling for three control functions with $\alpha = 3$ (the blue diamond), 0.6 (green triangle), and 1 (red circle). (b) The parameter Λ in Eq. (6) as the function of the power index α. The experimental results, represented by the red diamond, are obtained by fitting the relation of $W^{(\mathrm{ir})} \sim 1/M$. The theoretical curve in Eq. (6) is plotted with the green dash-dotted line.

tuning of irreversible entropy generation via adjusting the mode of operation is meaningful for the design of heat engines with high output power and efficiency.

Conclusion.—We have designed the apparatus with the cylinder-gas system to test the theoretically predicted $1/\tau$ scaling of the irreversible entropy generation at the long-time regime in the finite-time thermodynamics. Our experiment for the first time directly shows that the irreversible entropy generation, obtained by measuring the irreversible work, is inversely proportional to the process time τ in the long-time regime [Fig. 2(b)], namely, $\Delta S^{(\mathrm{ir})} \propto 1/\tau$. It is worth mentioning that the experimental obtained results also show a clear deviation from the $1/\tau$ scaling at the short-time regime; such phenomenon needs further theoretical and experimental exploration. Moreover, we demonstrated the proportional relation between entropy generation and the speed fluctuation of the piston with different gas compression schemes for the discrete quasi-isothermal process. Specifically, we verified the minimal entropy generation can be achieved by pushing the piston linearly within the set of the power control functions. This provides a feasible and convenient solution for the optimization of the actual heat engine by applying different control schemes to the work substance in different processes of the thermodynamic cycle.

The similar detection of the irreversible work can potentially be realized in several quantum systems, such as trapped ions [47–49], nuclear magnetic resonance system [50], Bose-Einstein condensate [51], and superconducting circuit systems [52,53]. The generalization of the current measurement in quantum regime could show the influence of coherence on these thermodynamic quantities [54–56].

Y.-H. M. is grateful to Hong Yuan for helpful discussions. We would like to thank the anonymous referees for helpful suggestions on the discussions of the short-time deviations. This work is supported by the National Natural Science Foundation of China (NSFC) (Grants No. 11534002, No. 11875049, No. U1930402, and No. U1930403), and the National Basic Research Program of China (Grants No. 2016YFA0301201)

*hdong@gscaep.ac.cn

[1] K. Huang, *Introduction To Statistical Physics*, 2nd ed. (T&F/CRC Press, Boca Raton, 2013), ISBN .
[2] M. Esposito, U. Harbola, and S. Mukamel, Rev. Mod. Phys. **81**, 1665 (2009).
[3] M. Campisi, P. Hänggi, and P. Talkner, Rev. Mod. Phys. **83**, 771 (2011).
[4] J. P. Pekola, Nat. Phys. **11**, 118 (2015).
[5] S. Vinjanampathy and J. Anders, Contemp. Phys. **57**, 545 (2016).
[6] *Thermodynamics in the Quantum Regime*, edited by F. Binder, L. A. Correa, C. Gogolin, J. Anders, and G. Adesso (Springer International Publishing, New York, 2018).
[7] C. M. Bender, D. C. Brody, and B. K. Meister, J. Phys. A **33**, 4427 (2000).
[8] T. E. Humphrey, R. Newbury, R. P. Taylor, and H. Linke, Phys. Rev. Lett. **89**, 116801 (2002).
[9] H. T. Quan, Y. X. Liu, C. P. Sun, and F. Nori, Phys. Rev. E **76**, 031105 (2007).
[10] Y.-H. Ma, S.-H. Su, and C.-P. Sun, Phys. Rev. E **96**, 022143 (2017).
[11] F. L. Curzon and B. Ahlborn, Am. J. Phys. **43**, 22 (1975).
[12] P. Salamon, A. Nitzan, B. Andresen, and R. S. Berry, Phys. Rev. A **21**, 2115 (1980).
[13] K. Sekimoto and S. ichi Sasa, J. Phys. Soc. Jpn. **66**, 3326 (1997).
[14] C. V. den Broeck, Phys. Rev. Lett. **95**, 190602 (2005).
[15] Z. C. Tu, J. Phys. A **41**, 312003 (2008).

[16] M. Esposito, R. Kawai, K. Lindenberg, and C. van den Broeck, Phys. Rev. Lett. **105**, 150603 (2010).
[17] B. Andresen, P. Salamon, and R. S. Berry, Phys. Today **37**, No. 9, 63 (1984).
[18] J. Chen, J. Phys. D **27**, 1144 (1994).
[19] A. Ryabov and V. Holubec, Phys. Rev. E **93**, 050101(R) (2016).
[20] V. Holubec and A. Ryabov, Phys. Rev. E **96**, 062107 (2017).
[21] V. Holubec and A. Ryabov, J. Stat. Mech. (2016) 073204.
[22] N. Shiraishi, K. Saito, and H. Tasaki, Phys. Rev. Lett. **117**, 190601 (2016).
[23] V. Cavina, A. Mari, and V. Giovannetti, Phys. Rev. Lett. **119**, 050601 (2017).
[24] Y.-H. Ma, D. Xu, H. Dong, and C.-P. Sun, Phys. Rev. E **98**, 042112 (2018).
[25] Z.-C. Tu, Chin. Phys. B **21**, 020513 (2012).
[26] M. H. Rubin, Phys. Rev. A **19**, 1272 (1979).
[27] B. Sahin, A. Kodal, and H. Yavuz, Energy **21**, 1219 (1996).
[28] Y. Wang and Z. C. Tu, Phys. Rev. E **85**, 011127 (2012).
[29] J. Stark, K. Brandner, K. Saito, and U. Seifert, Phys. Rev. Lett. **112**, 140601 (2014).
[30] I. Derényi and R. Astumian, Phys. Rev. A **59**, R6219 (1999).
[31] T. Schmiedl and U. Seifert, Europhys. Lett. **81**, 20003 (2007).
[32] Y. Izumida and K. Okuda, Europhys. Lett. **83**, 60003 (2008).
[33] U. Seifert, Rep. Prog. Phys. **75**, 126001 (2012).
[34] A. Dechant, N. Kiesel, and E. Lutz, Phys. Rev. Lett. **114**, 183602 (2015).
[35] C. de Tomás, A. C. Hernández, and J. M. M. Roco, Phys. Rev. E **85**, 010104(R) (2012).
[36] Y.-H. Ma, D. Xu, H. Dong, and C.-P. Sun, Phys. Rev. E **98**, 022133 (2018).
[37] See Supplemental Material at http://link.aps.org/supplemental/10.1103/PhysRevLett.125.210601 for the derivation of Eqs. (4) and (6), detailed discussion on the relaxation time t_r, and additional results from pressure sensors $S2$ and $S3$.
[38] D. E. Krause and W. J. Keeley, Phys. Teach. **42**, 481 (2004).
[39] C. T. O' Sullivan, Am. J. Phys. **58**, 956 (1990).
[40] Y. Izumida and K. Okuda, Phys. Rev. E **96**, 012123 (2017).
[41] B. Andresen, R. S. Berry, A. Nitzan, and P. Salamon, Phys. Rev. A **15**, 2086 (1977).
[42] H. T. Quan, S. Yang, and C. P. Sun, Phys. Rev. E **78**, 021116 (2008).
[43] G. E. Crooks, Phys. Rev. Lett. **99**, 100602 (2007).
[44] E. Geva and R. Kosloff, J. Chem. Phys. **96**, 3054 (1992).
[45] Z. Gong, Y. Lan, and H. T. Quan, Phys. Rev. Lett. **117**, 180603 (2016).
[46] D. S. P. Salazar, Phys. Rev. E **101**, 030101(R) (2020).
[47] O. Abah, J. Roßnagel, G. Jacob, S. Deffner, F. Schmidt-Kaler, K. Singer, and E. Lutz, Phys. Rev. Lett. **109**, 203006 (2012).
[48] S. An, J.-N. Zhang, M. Um, D. Lv, Y. Lu, J. Zhang, Z.-Q. Yin, H. Quan, and K. Kim, Nat. Phys. **11**, 193 (2015).
[49] J. Rossnagel, S. T. Dawkins, K. N. Tolazzi, O. Abah, E. Lutz, F. Schmidt-Kaler, and K. Singer, Science **352**, 325 (2016).
[50] R. J. de Assis, T. M. de Mendonça, C. J. Villas-Boas, A. M. de Souza, R. S. Sarthour, I. S. Oliveira, and N. G. de Almeida, Phys. Rev. Lett. **122**, 240602 (2019).
[51] M. Brunelli, L. Fusco, R. Landig, W. Wieczorek, J. Hoelscher-Obermaier, G. Landi, F. L. Semião, A. Ferraro, N. Kiesel, T. Donner *et al.*, Phys. Rev. Lett. **121**, 160604 (2018).
[52] F. Giazotto, T. T. Heikkilä, A. Luukanen, A. M. Savin, and J. P. Pekola, Rev. Mod. Phys. **78**, 217 (2006).
[53] R. Uzdin and N. Katz, arXiv:1908.08968.
[54] K. Brandner, M. Bauer, and U. Seifert, Phys. Rev. Lett. **119**, 170602 (2017).
[55] S. Su, J. Chen, Y. Ma, J. Chen, and C. Sun, Chin. Phys. B **27**, 060502 (2018).
[56] P. A. Camati, J. F. G. Santos, and R. M. Serra, Phys. Rev. A **99**, 062103 (2019).